**Drugs against *Mycobacterium tuberculosis* 3-isopropylmalate dehydrogenase can be developed using homologous enzymes as surrogate targets**

Éva Gráczer[§], András Bacsó[§], Dénes Kónya[#], Adrián Kazi[#], Tibor Soós[#], Laura Molnár[#], Tamás Szimler[§], László Beinrohr[§], András Szilágyi[§], Péter Závodszky[§] and Mária Vas[§,*]

[§]Institute of Enzymology, Research Centre for Natural Sciences, Hungarian Academy of Sciences, H-1117 Budapest, Magyar tudósok körútja 2., Hungary

[#]Institute of Organic Chemistry, Research Centre for Natural Sciences, Hungarian Academy of Sciences, H-1117 Budapest, Magyar tudósok körútja 2., Hungary

[*]*Corresponding author*:

Mária Vas

Institute of Enzymology, Research Centre for Natural Sciences, Hungarian Academy of Sciences

H-1117 Budapest, Magyar tudósok körútja 2., Hungary

H-1519 Budapest, P. O. Box 286., Hungary

Tel.: 36 1 3826 773

E-mail: vas.maria@ttk.mta.hu

**RUNNING TITLE:** *Mycobacterium tuberculosis* 3-isopropylmalate dehydrogenase

**ABSTRACT**

3-Isopropylmalate dehydrogenase (IPMDH) from *Mycobacterium tuberculosis* (*Mtb*) may be a target for specific drugs against this pathogenic bacterium. We have expressed and purified *Mtb* IPMDH; and determined its physico-chemical and enzymological properties. Size-exclusion chromatography and dynamic light scattering measurements (DLS) suggest a tetrameric structure for *Mtb* IPMDH, in contrast to the dimeric structure of most of the IPMDHs. The kinetic properties ($k_{cat}$ and $K_m$ values) of *Mtb* IPMDH and the pH-dependence of $k_{cat}$ are very similar to both *Escherichia coli* (*Ec*) and *Thermus thermophilus* (*Tt*) IPMDHs. The stability of *Mtb* IPMDH in 8 M urea is close to that of the mesophilic counterpart, *Ec* IPMDH, both of them being much less stable than the thermophilic (*Tt*) enzyme. Two known IPMDH inhibitors, O-methyl oxalohydroxamate and 3-methylmercaptomalate, have been synthesised. Their inhibitory effects were found to be independent of the origin of IPMDHs. Thus, experiments with either *Ec* or *Tt* IPMDH would be equally relevant for designing specific inhibitory drugs against *Mtb* IPMDH.

**KEYWORDS**: enzyme kinetics, expression, isopropylmalate dehydrogenase, inhibition, *Mycobacterium tuberculosis*, purification, physico-chemical characterisation

3-Isopropylmalate dehydrogenase (IPMDH) is an essential enzyme in the leucine biosynthesis pathway of bacteria and plants, but it is absent in humans and other mammals. Various *in vivo* and *in vitro* studies demonstrate that those pathogenic bacterium strains that cannot synthesize leucine are unable to replicate inside their host cells [1-3]. The lack of the leucine biosynthetic pathway in humans (and generally in mammals) suggests that enzymes of this pathway, such as IPMDH, may serve as potential targets for inhibition by specific new drugs against pathogenic bacteria such as *Mycobacterium tuberculosis*. This bacterium is the major causative agent of tuberculosis, a potentially lethal disease that causes 2-3 million deaths per year, globally. Due to the frequent appearance of resistance against current antibiotics, there is an urgent need to find potential new drug targets and design more effective drugs. IPMDH, one of the catalysts of leucine biosynthesis, seems to be an appropriate target for inhibition by small-molecule drugs. Designing new inhibitory molecules against IPMDH, however, requires detailed knowledge of the structure and catalytic mechanism of this enzyme.

IPMDH catalyses the complex reaction of simultaneous oxidation and decarboxylation of the substrate 3-isopropylmalate (IPM) in the presence of $NAD^+$. For the catalytic reaction, the presence of a divalent metal ion ($Mn^{2+}$ or $Mg^{2+}$) is also required. Our knowledge on the kinetics and mechanisms on IPMDH is limited [4-7]. Efforts have been mainly concentrated on revealing the molecular basis of thermostability [8-11]. There are also numerous crystallographic structural investigations of IPMDHs from various sources [12-19].

Briefly, IPMDHs, in general, have a characteristic homodimer structure [20, 21] and each subunit can be divided into two domains. The substrate, MnIPM, binds at the interface between the domains and at the same time this site is located at the subunit-subunit interface. Thus, IPM binding requires special attention with respect to regulation of both domain-domain and subunit-subunit interactions. In fact, the MnIPM-bound IPMDH exists in a presumably active, domain-closed conformation [14, 19]. A detailed atomic-level mechanism of domain closure has also been described for *Thermus thermophilus* (*Tt*) IPMDH from structural analysis [19]. The crystal structure of *Mycobacterium tuberculosis* (*Mtb*) IPMDH is the only one in which the apo- (substrate-free) protein appeared in a largely closed conformation [18]. As discussed previously, the different behaviour may be due to the specific crystallisation conditions used for structure determination or may be attributed to some species-specific differences in the structures of various IPMDHs.

Therefore, in the present work, we aimed to produce *Mtb* IPMDH in pure homogeneous form in order to characterize its enzymological and physico-chemical properties, and furthermore, to compare it with its better-characterised counterparts, the thermophilic *Thermus thermophilus* (*Tt*) and the mesophilic *Escherichia coli* (*Ec*)

IPMDHs. Although sequence comparisons indicate extensive differences, we found that these differences are not associated with significantly different enzyme kinetic and physico-chemical properties.

## MATERIALS and METHODS

### *Chemicals and Enzymes*

The substrate, 3-isopropylmalate (IPM) or (2*R*,3*S*)-2-hydroxy-3-(propan-2-yl) butanedioic acid was purchased in the racemic DL-threo form from Wako Biochemicals (Japan), $NAD^+$ and NADH were Sigma products. All other chemicals were commercially available high purity reagent grade products.

The inhibitory compounds, O-methyl oxalohydroxamate and 3-methylmercaptomalate or (2*S*,3*S*)-(-)-2-hydroxy-3-sulfanylbutanedioic acid (in the form of the racemic mixture of trans-2-hydroxy-3-sulfanylbutanedioic acid) were synthesised chemically by using the previously described methods by Pirrung [22] and Nango *et al.* [23], respectively. The purity of the synthesised products was at least 90 % as determined by NMR measurements and elementary analysis.

Wild-type *Tt* and *Ec* IPMDHs were expressed in *Ec* BL21 DE3 pLysS strain, purified and stored as described previously [9, 10]. Their concentration (in molarity of the monomers) was calculated using $\varepsilon_{280}$ values of 23950 and 27390 $M^{-1}cm^{-1}$ for *Tt* and *Ec* IPMDHs, respectively. *Mtb* IPMDH was overexpressed in *Ec* BL21 cc3 cells [24], transformed with pETM-11-*leuB* vector [18] in two different ways. First, *Mtb* IPMDH was expressed using the usual method of batch techniques. This method, however, resulted in mostly insoluble IPMDH in the form of inclusion bodies, from which the active enzyme could not be renaturated. The amount of soluble IPMDH protein in the supernatant was negligible. Finally, a fermentation procedure allowing control of cultivation parameters has been used for protein expression. The cells from an overnight pre-culture containing the plasmid pETM-11 with *Mtb* IPMDH gene were grown in minimal medium containing 13.3 g/L $KH_2PO_4$, 1.2 g/L $MgSO_4 \cdot 7\ H_2O$, 30 g/L glycerol, 1.7 g/L citric acid, 4 g/L $(NH_4)_2HPO_4$, 8.4 mg/L EDTA, trace metal ions and antibiotics (17 mg/L chloramphenicol, 50 mg/L kanamycin, 50 mg/L spectinomycin) at 30 $^oC$, pH=7, stirring speed 950 rpm and 1.5 L/min airflow. After the initial amount of carbon source was consumed, a feed-batch phase was followed for 4 hours. The feeding solution (1000 g/L glycerol, 20 g/L $MgSO_4 \cdot 7\ H_2O$ and trace metal ions) was added at a rate to keep the dissolved oxygen levels at ~20%. Just before the end of this fed-batch phase, the temperature was lowered to 20 $^oC$ and the expression was induced by the addition of isopropyl β-D-thiogalactopyranoside (1.4 mM final concentration). At the same time yeast extract solution (2 g/L final

concentration) was also added. The induction procedure was repeated after 1.5 hours. After the first induction step, the culture was incubated for about 3 hours and then harvested. The cells were lysed using sonication in a buffer containing 10 mM imidazole, 50 mM $NaH_2PO_4$, pH=8.0 and 300 mM NaCl for 20 minutes with 25 second pulses on ice. The cell debris was pelleted by centrifugation for 30 minutes at 4 $^oC$ and 18000 rpm. The supernatant was loaded onto a Ni-NTA column (8 mL volume) equilibrated with 50 mM imidazole, 50 mM $NaH_2PO_4$, pH=8.0, 300 mM NaCl buffer. The protein was eluted by a linear gradient from 50 mM to 500 mM imidazole buffer in a total volume of 100 mL. The peak fractions were dialysed overnight against 25 mM MOPS-KOH buffer pH=7.6 and concentrated to ~5 mg/mL. The protein concentration has been determined by using an apparent molar absorption coefficient of $\varepsilon_{280}$(app)=16941 $M^{-1}$ $cm^{-1}$ which was obtained by correction of the theoretically calculated value of $\varepsilon_{280}$=15930 $M^{-1}$ $cm^{-1}$ for the monomer [25] by the additional absorbance of a bound nucleotide (cf. Results). The yield of *Mtb* IPMDH from 1.5 L cell culture was ~8-10 mg. The purity of the protein (at least 95 %) was estimated by SDS-PAGE.

*SDS-, native- and urea gel electrophoresis*

SDS gel electrophoresis was carried out using the method of Laemmli [26]. Native gel electrophoresis was performed according to Ornstein [27]. The resolving and stacking gel was 10% and 5%, respectively. IPMDH (3-5 μg) was loaded into the gel, and the electrophoresis was carried out at 180 V for 1 h. The urea gel electrophoresis was performed similarly to the native gel electrophoresis, but all solutions contained 8 M urea and the samples of IPMDH also were denaturated in 8 M urea. The gels were stained with Coomassie Brilliant Blue G-250.

*Gel filtration chromatography*

A superose 12 HR 10/30 column from Pharmacia LKB Biotechnology was used to determine the molecular weight of the native *Tt*, *Ec* and *Mtb* IPMDHs. The column was equilibrated with 25 mM MOPS-KOH pH=7.6 buffer and the flow rate was set to 0.5 mL/min. 100 μL of the IPMDH samples (concentration 1.2 mg/mL) were injected into the column and the eluted proteins were detected at 280 and 260 nm.

*Dynamic Light Scattering (DLS) measurements*

The molecular sizes of the various IPMDHs were tested with a DynaPro Titan Temperature Controlled Micro Sampler (Wyatt Technology Corporation, U.S.) instrument equipped with a laser (power 2%) operating at 830

nm. Samples of IPMDHs with final protein concentration of 8.3 mg/mL were prepared in 25 mM MOPS-KOH buffer, pH 7.6 and filtered through a Millipore filter (pore size 0.1 μm). A quartz microcell (12 μl) with a 1.5 mm light path was used and the scattered light intensities were collected at an angle of 90°. Each data set were collected for 20s and repeated 25 times at 21°C. The data were evaluated by the aid of Dynamics V6 (tm) Version 6.10.0.10 software using the Isotropic Spheres Model and the Regularization Fit. The size distribution of all the investigated samples were effectively monomodal, i.e. the larger aggregates were insignificant. In addition, the samples were found to be monodisperse.

*Enzyme activity measurements*

Activity of IPMDH (6-12 μg/mL, i.e., 0.16-0.32 μM monomer) usually was assayed in the presence of the substrates IPM, $MnCl_2$ and $NAD^+$ as well as 10 mM DTT in 25 mM MOPS-KOH buffer (pH=7.6). In each series of experiments the concentration of one of the substrates was varied and the other ones were kept constant, close to the saturating value (0.5 mM IPM, 0.5 mM $MnCl_2$ or 3 mM $NAD^+$). Alternatively, the substrate IPM was replaced by the analogue 3-methylmercaptomalate, named as (2*S*,3*S*)-(-)-2-hydroxy-3-sulfanylbutanedioic acid according to the IUPAC nomenclature. In the inhibitory studies activity was measured at different (in each case constant) concentrations of inhibitor and at varying concentration of the substrate, IPM. Formation of NADH was recorded spectrophotometrically at 340 nm ($\varepsilon_{340}$ = 6220 $M^{-1}$ $cm^{-1}$), at 20 °C, using a Jasco (Tokyo, Japan) V-550 spectrophotometer equipped with a Grant Y6 thermostat. The experimental activity values of the substrate saturation curves have been fitted to the Michaelis-Menten equation and yielded the $V_{max}$ and the $K_m$ values. From the $V_{max}$ values the molar activities of *Tt*, *Ec* and *Mtb* IPMDH subunits at pH=7.6 have been derived to be 238 ± 30, 700 ± 80 and 200 ± 20 $min^{-1}$, respectively. When $MgCl_2$ (2 mM) replaced $MnCl_2$ the molar activities of all IPMDHs were reduced by about 50%. The results of the inhibitory studies have been evaluated in a double reciprocal Lineweaver-Burk plot.

The activity was also tested at different pH-s using the buffers 25 mM MOPS (pH 6.0-8.0), 10 mM HEPES (pH 6.8-8.1), 50 mM Tris-HCl (pH 7.1-9.0), 50 mM diethanolamine (pH 7.7-10.8), 25 mM 1,2-diaminoethane (pH 9.0-11.0). The overlapping pH-ranges of the particular buffers assured elimination of any influence of the specific buffer components on the enzyme activity. In each case the activity was measured at two different substrate concentrations close to saturation and these values were averaged. The experimental activity values as a function of pH were fitted according to the Henderson-Hasselbach equation of a simple deprotonation dissociation curve:

$$\nu_{measured} = \frac{\nu_{extrapolated}}{1+10^{-(pH-pK)}} \qquad \text{Eq. 1.}$$

where $v_{measured}$: the activity value measured at a given pH

$v_{extrapolated}$: the maximal activity value extrapolated to the high pH-range

*pK*: characteristic of a catalytic dissociating side-chain

*UV absorbance, CD and fluorescence spectral measurements*

UV absorbance was recorded in the range of 240 and 350 nm using a Jasco V-550 (Tokyo, Japan) spectrophotometer equipped with a Grant Y6 thermostat. The absorbance of proteins was measured in a cuvette with 1 mm path length and at 2 nm bandwidths.

CD measurements were performed with a Jasco J-720 spectropolarimeter equipped with a Neslab RTE 111 computer-controlled thermostat. For recording the far-UV CD spectra, the cuvette with 1 mm path length was used at a protein concentration of 0.6 mg/mL (15 μM monomer).

The protein fluorescence spectra were recorded using a SPEX (Edison, NJ) Fluoromax-3 spectrofluorimeter equipped with a Peltier thermostat. The samples were excited at 295 nm, and the emission was monitored between 300 and 400 nm using the cuvette with a 10 mm path length. Slits were 2 nm and 4 nm wide for excitation and emission, respectively. All measurements were carried out at 20 $^{o}$C.

*FRET experiments*

The Förster resonance energy transfer (FRET) between the Trp(s) of IPMDH and the bound NADH was recorded at 20 $^{o}$C in the presence of $Mg^{2+}$ and IPM as reported by Dean and Dvorak [4] using a SPEX Fluoromax-3 spectrofluorimeter equipped with a Peltier thermostat (Edison, NJ). The usual mixture contained 12 μg/mL (0.32 μM monomer) IPMDH, 12.5 μM NADH, 3 mM $MgCl_2$ and 0.5 mM IPM. Alternatively, IPM was replaced by the substrate analogue (*2S,3S*)-(-)-3-methylmercaptomalate. The protein was excited at 295 nm and the emission by the bound NADH was recorded between 300 and 540 nm in a cuvette with 10 mm path length. The slits of 2 and 4 nm were applied for excitation and emission, respectively.

IPM or analogue binding to the complex of native IPMDHs (*Tt* and *Mtb*) with NADH and $Mg^{2+}$ was detected by fluorimetric titration using the signal of FRET occurring between the protein Trp(s) and the bound NADH, upon addition of increasing concentrations of the substrate/analogue. The equation used for calculation of $K_d$ of the IPM/analogue-binding:

$$I_{measured}=I_{max}*[S]/(K_d+[S])$$ Eq. 2

Where $I_{measured}$ is the fluorescence intensity recorded at different substrate concentrations

$I_{max}$ is the fluorescence intensity extrapolated to infinite substrate concentrations

[S] is the molar concentration of the substrate

$K_d$ is the dissociation constant

*Denaturation of IPMDH monitored by protein fluorescence measurements*

Denaturation of *Mtb* IPMDH was initiated by dilution into a solution containing 8 M urea, 25 mM MOPS-KOH buffer (pH=7.6). Time courses of unfolding were followed at 20 °C by monitoring the changes in protein fluorescence. The protein concentration in the denaturation experiments was 12 μg/mL (0.32 μM, monomer). The experiments were carried out both in the absence of substrates and in the presence of 0.6 mM IPM and 0.6 mM $MnCl_2$. For fluorescence the samples were excited at 295 nm, and the emission spectra were recorded in every 5 minute between 300 and 400 nm using a cuvette with 10 mm path length. The slits were set to 2-4 nm for excitation and emission. The fluorescence intensities at 335 nm and the $\lambda_{max}$ (the wavelengths at maximum protein fluorescence intensity) were plotted at different time intervals during denaturation. The time-dependent curves of protein denaturation were fitted by a single exponential equation.

*Renaturation of IPMDH followed by ANS fluorescence and by enzyme activity measurements*

The concentration of ANS was determined using $\varepsilon_{350}$ = 4954 $M^{-1}$ $cm^{-1}$ [28] in water. For renaturation studies, denatured *Mtb* IPMDH were prepared at protein concentrations of 600 μg/mL (8.15 μM) upon incubation for 1 h in 25 mM MOPS-KOH buffer, pH=7.6, containing 8 M urea. Refolding experiments were initiated by 100-fold dilution of the denatured protein into the MOPS buffer containing ANS that was present in the renaturation mixture in a 200-fold molar excess over IPMDH. The excitation wavelength was 350 nm, and refolding kinetics was followed at 480 nm. The slits for both excitation and emission were 4 nm.

Refolding followed by enzyme activity measurements was initiated by direct dilution the denatured protein into the activity assay solution. During the reactivation process formation of NADH was continuously recorded at 340 nm. The activity values at various time intervals of renaturation have been obtained by derivation of this curve at various times.

*Sequence comparison and alignment*

Protein sequences of various bacterial IPMDHs were downloaded from the Uniprot database (www.uniprot.org/uniprot). The sequences were compared using the algorithm downloaded from http://www.ebi.ac.uk/Tools/psa/emboss_needle.

The alignment of IPMDH sequences from various origins was first carried out by the software BioEdit. These alignments were checked using the molecular graphics software Insight II 95.0 (Biosym/MSI, San Diego, CA, USA) and were corrected manually, if required.

*Comparison of some structural features of the investigated IPMDHs*

Identification of the atomic contacts of the non-conserved amino-acid residues of *Mtb* IPMDH with the conserved ones were carried out using the X-ray coordinates of the crystal structure (pdb: 1W0D) with Insight II, as described earlier [19].

The possible binding modes of the substrates, $Mn^{2+}$-complex of IPM and $NAD^{+}$, to *Mtb* IPMDH have been determined by molecular graphical modelling based on the known crystal structures of *Tt* IPMDH (pdb codes 2Y41 and 2Y42) [19].

The extent of hydrophobic surface area of the three investigated IPMDHs was calculated from their pdb coordinates using the software ALPHASURF [29].

Prediction of the energetically stable oligomeric states of the three IPMDHs was carried out using the PISA server [30].

The isoelectric points and the molecular charges of the three investigated IPMDHs was estimated by the PROPKA software [31].

## RESULTS and DISCUSSION

### Expression of *Mtb* IPMDH by fermentation and its molecular size

Fig. 1A illustrates various stages of expression of *Mtb* IPMDH by SDS-PAGE. The last sample is the purified enzyme obtained after the Ni-affinity chromatography. This run clearly confirms the purity (at least 95%) of the produced *Mtb* IPMDH. The yield was 8-10 mg protein from 1.5 litres of cell culture.

Comparative native gel electrophoresis of *Tt*, *Ec* and *Mtb* IPMDHs is shown in Fig. 1B. Surprisingly, the electrophoretic mobility of *Mtb* IPMDH was much lower compared to the other two IPMDHs. Considering the closely similar isoelectric points of the three IPMDHs as calculated using PROPKA [31] (pI=6.0 for both *Tt* and *Mtb*, pI=5.66 for *Ec* IPMDH) the much lower mobility of *Mtb* IPMDH would not be expected. Therefore, this experiment raised the possibility that *Mtb* IPMDH has a larger molecular size (e.g. higher degree of association of its polypeptide chains). In order to test this assumption, we have repeated the electrophoresis in the presence of 8 M urea (Fig. 1D). Under this condition, the polypeptide chains become dissociated and unfolded. However, their electrophoretic mobilities are still influenced by their charges at the pH of the running buffer. We have estimated using PROPKA [31] that the chains of *Tt*, *Mtb* and *Ec* possess the following net charges at pH 9.0 (i.e. at the pH of the electrophoresis): -9.8, -14.4 and -20.3, respectively. Thus, the electrophoretic mobilities of the three enzymes in 8 M urea should follow the order of their charges. Indeed, as shown by Fig. 1D, the three enzymes with similar denatured states showed running rates, with the *Mtb* enzyme being between the *Tt* and *Ec* IPMDHs. Thus, the slight differences in the charges of the IPMDH molecules cannot explain the observed retarded electrophoretic mobility of the *Mtb* IPMDH on the native gel (Fig. 1B). These observations are in accordance with the assumption of a different quaternary structure of *Mtb* IPMDH, possibly a higher oligomerisation state. Therefore, we have carried out size exclusion chromatography under native conditions with the three investigated IPMDHs. As illustrated in Fig. 1C, the apparent molecular weights of *Tt*, *Ec* and *Mtb* IPMDHs were obtained to be about 64 kDa, 66 kDa and 89 kDa, respectively. For *Tt* and *Ec* IPMDHs, a dimeric structure has been confirmed [13, 20], and their molecular masses are approximately 76 kDa, i.e. somewhat higher than the presently obtained experimental values (64-66 kDa). Thus, it is possible that the experimentally determined elution volumes are perturbed due to the non-spherical shape of the molecule. Therefore, the estimated increased molecular mass of *Mtb* IPMDH likely reflects a tetrameric structure, since a trimeric structure would be inconsistent with the symmetry properties of the molecule. A similar gel-filtration

experiment with *Sulfolobus* sp. strain 7 IPMDH also suggested an oligomeric state only slightly higher than a dimer [32] and its tetrameric state has indeed been demonstrated later by analytical ultracentrifugation [33].

To confirm the oligomerisation states of the IPMDHs used in the present work, we have also carried out comparative DLS studies. The predicted apparent hydrodynamic radii of *Tt*, *Ec* and *Mtb* IPMDHs were obtained to be 29.8±2, 31.5±1 and 43±2 Å, in the same order. The value for the *Tt* enzyme agrees well with the gyration radius of 28.7±0.3 Å determined earlier by small angle X-ray scattering [6]. These results are in agreement with the assumed higher oligomerisation state of *Mtb* IPMDH. Using DLS we have also found that various nucleotides (dNTP mixture, $NAD^+$, ATP), possibly present during bacterial expression, do not affect the values of hydrodynamic radii.

Using the crystallographic structure of *Mtb* IPMDH (PDB entry 1W0D) we predicted the likely oligomerisation state of the protein using the PISA server [30] which generates all possible oligomerisation states by symmetry operations and selects the most likely state by calculating buried surfaces and estimating dissociation free energies. Based on these calculations, the most likely oligomerisation state was predicted to be a tetramer (Fig. 2). This tetramer appears to be a weakly associated dimer of two more strongly associated dimers, with an estimated dissociation free energy of 12.4 kcal/mol for the dissociation of the tetramer into two dimers and 40.6 kcal/mol for the dissociation of each dimer into monomers. The interface between the two dimers is also smaller (2685 $Å^2$) and less hydrophobic (~60% apolar) than the interfaces between the monomers in the dimers (~4300 $Å^2$ each, ~68% apolar) as calculated by the program ALPHASURF [29]. The same type of modelling for the *Tt* IPMDH predicted even smaller (2062 $Å^2$) and less hydrophobic (~54%) hypothetical interface between the dimers. (The available crystal structure of the dimeric *Ec* IPMDH that exhibits a different conformation, however, did not allow to carry out similar modelling.)

In the predicted tetrameric structure of *Mtb* IPMDH, it is peculiar that the arms of each subunit are important not only for the stabilization of the dimers, but also for maintaining the tetrameric structure. It is also notable that the substrate binding sites (illustrated below on Fig. 8) are not perturbed or shielded by the oligomeric contacts. Thus, the catalytic efficiency of the enzyme is possibly not changed in the tetrameric state, i.e. the biological relevance of the enzyme is most probably not dependent on the dimer-tetramer transition.

**Spectral properties of *Mtb* IPMDH in comparison with *Tt* and *Ec* IPMDHs**

Since certain structural characteristics of proteins are often reflected by their spectral properties, we first recorded the UV spectrum of *Mtb* IPMDH and compared it to its *Tt* and *Ec* counterparts (Fig. 3A). Surprisingly,

in contrast to the other two enzymes, the absorption maximum of *Mtb* IPMDH is not at 280 nm but shifted somewhat towards the lower wavelengths. Thus, in contrast to the ratio of $A_{280}/A_{260}$=1.6, characteristic of other IPMDHs, this ratio is only 0.8 in the case of *Mtb* IPMDH. We assumed that the latter enzyme binds some nucleotide that is most probably $NAD^+$. In order to test this possibility, we have added the other substrate IPM and $Mn^{2+}$ (at closely saturating concentrations, cf. Methods) to the enzyme, but no NADH formation could be detected. Therefore, we can only conclude that some other unidentified nucleotide of the cell remains bound to the enzyme, in spite of the isolation procedure. The existence of a nucleotide in this solution was shown by the spectrum (grey solid line) with $\lambda_{max}$=260 nm obtained after removal of the protein by heat denaturation and centrifugation of the precipitate. When this spectrum of the nucleotide was subtracted from the original spectrum of the native *Mtb* IPMDH (dotted), the spectrum of the nucleotide-free *Mtb* IPMDH (black solid line) can be obtained. Taking into account the ratio of the $A_{280}$ values of the spectra of dotted and black solid lines at 280 nm, the theoretical molar absorption coefficient of *Mtb* IPMDH ($\varepsilon_{280}$=15930 $M^{-1}$ $cm^{-1}$ for the monomer [25]) can be corrected and obtained to be $\varepsilon_{280}$(app.)=16941 $M^{-1}cm^{-1}$. Furthermore, the binding of the nucleotide to *Mtb* IPMDH is probably not very tight, as it can be removed from the protein by gel filtration (not shown).

The far-UV CD spectra of *Mtb*, *Tt*, and *Ec* IPMDHs are compared in Fig. 3B. As expected, the molar ellipticity values, characteristic of the three proteins are very similar to each other. Thus, the amounts and the qualities of the secondary structural elements in all three proteins are very similar to each other, as suggested by the similarities of their X-ray structures [13, 18, 19].

The protein fluorescence emission spectra of *Mtb*, *Ec* and *Tt* are shown in Fig 3C. The emitted fluorescent intensities are seemingly proportional to the Trp content of the three proteins: *Mtb*, *Ec* and *Tt* IPMDHs contain 1, 2 and 3 Trp side-chains per mole subunits, respectively. However, the characteristic $\lambda_{max}$ values of the spectra are slightly different, possibly due to the different chemical environments of the Trp side-chains in the three different proteins.

A special fluorescent phenomenon, FRET, exhibited by all the investigated IPMDHs is illustrated in Fig. 3D. The occurrence of this Förster (F) resonance (R) energy (E) transfer (T) has been observed with *Tt* IPMDH from its Trp side-chains to the nicotinamide ring of the bound NADH when the other substrate IPM is also bound [4]. It was shown that the presence of the metal ion $Mn^{2+}$ or $Mg^{2+}$ is also essential for this phenomenon [6]. It is reasonable to assume that the conformational changes caused by the binding of IPM (possibly associated with the domain closure) bring the NADH nicotinamide and the Trp indole rings in a relative orientation optimal for the occurrence of FRET. It is seen in Fig. 3D that increasing fluorescent intensity

of the bound NADH is accompanied by decreasing protein fluorescence intensity for all three enzymes. Thus, *Mtb* IPMDH exhibits the FRET phenomenon, similarly to the other two IPMDHs.

It may be notable that similar FRET spectra (although with somewhat lower intensities) were obtained when IPM was replaced by the substrate analogue (2*S*,3*S*)-(-)-3-methylmercaptomalate (cf. below) for both the *Tt* and *Mtb* IPMDHs (not shown).

**Enzyme kinetic parameters of *Mtb* IPMDH in comparison with *Tt* and *Ec* IPMDHs**

Activity of *Mtb* IPMDH was tested at varying concentrations of each substrate. The kinetic constants derived from the the substrate saturation curves by fitting according to the Michaelis-Menten equation, are summarised in Table 1, in comparison with those of *Tt* and *Ec* IPMDHs. The catalytic efficiencies of IPMDHs of the different origins are of similar magnitude. As for the $k_{cat}$ values, *Mtb* IPMDH exhibits a value comparable with the one characteristic of *Tt* IPMDH. On the other hand, the $K_m$ values of all three substrates are about 2-3 fold smaller for *Mtb* IPMDH, indicating its somewhat tighter interactions with the substrates, more similar to those of *Ec* IPMDH.

**Inhibitory effects of O-methyl oxalohydroxamate and (2*S*,3*S*)-(-)-2-hydroxy-3-sulfanylbutanedioic acid**

In order to find inhibitors against *Mtb* IPMDH, we have synthesized two different previously described compounds that were reported to be good inhibitors against *Tt* IPMDH. The compound O-methyl oxalohydroxamate [22] however, in our experiments (not shown) exhibited much weaker inhibitory properties towards *Tt* IPMDH ($K_I$=1.45±0.03 mM) compared to its previously reported value ($K_I$=1.2 μM). This is surprising because both data sets have been determined under closely similar experimental conditions. Thus, we decided to synthesize a recently published thia-analogue of IPM, 3-methylmercaptomalate or, according to the IUPAC nomenclature, (2*S*,3*S*)-(-)-2-hydroxy-3-sulfanylbutanedioic acid [23]. The intersecting double reciprocal Lineweaver-Burk plots of the kinetic data of the IPM saturation curves (Fig. 4A) in the absence and presence of the inhibitor clearly demonstrate the purely competitive character of the inhibition for both *Tt* and *Mtb* IPMDHs. The competitive inhibitory constants ($K_I$) are found to be closely similar, 349±50 nM and 427±50 nM, respectively, for these two different IPMDHs. These values are not very different from $K_I$=62 nM, determined earlier by Nango and coworkers with *Tt* IPMDH under somewhat different conditions but at much higher temperature, 60 $^{o}$C [23].

Further, Nango and coworkers reported that this substrate analogue inhibitor also exhibits a weak substrate activity, but it has not been quantified. In agreement with this finding, under our experimental conditions, we found $k_{cat}$ values as low as 1.2±0.2 $min^{-1}$ and 1.3±0.2 $min^{-1}$ for *Tt* and *Mtb* IPMDHs, respectively. The $K_m$ value of the analogue could not be quantified but was estimated to be in the nanomolar range.

**$K_d$ value of MnIPM binding to *Mtb* IPMDH in comparison with *Tt* and *Ec* IPMDHs**

As shown above (Fig. 3D), the FRET signal is formed only when IPM is bound to the enzyme. Thus the FRET signal is an indicator of IPM binding. Therefore, the enzyme could be titrated with IPM by detecting the increase of the FRET emission. The $K_d$ value of MnIPM binding to *Mtb* IPMDH in comparison with *Tt* and *Ec* IPMDHs has been obtained by fitting these titration curves to simple binding hyperbolas (cf. Methods) and the values are listed in Table 1. It is seen that the $K_d$ values are closely similar to the respective $K_m$ values of the substrate, in agreement with a rapid equilibrium enzyme kinetic mechanism.

**Formation of FRET spectrum in the presence of (2*S*,3*S*)-(-)-2-hydroxy-3-sulfanylbutanedioic acid and its binding parameters**

As noted above, FRET spectra of both *Tt* and *Mtb* IPMDHs are also formed with 3-methylmercaptomalate. This is not surprising because this compound is a weak substrate, thus, it may be able to induce conformational changes similar to those caused by the real substrate, IPM. Using this FRET signal, we have titrated both *Tt* and *Mtb* IPMDHs with this analogue in order to determine its binding constants (Fig. 4B). While for IPM, the binding constant ($K_d$) is in close agreement with its $K_m$ value (cf. Table 1), these two constants greatly differ for 3-methylmercaptomalate: while the $K_m$ values are in nanomolar range (cf. above), the $K_d$-values are in micromolar range (178±20 μM and 87±15 μM for *Tt* and *Mtb* IPMDHs, respectively). It is possible that the binding modes of this weak substrate are different in the presence of simultaneously bound $NAD^+$ (functioning complex) and NADH (non-functioning complex). These different binding modes might be reflected in these greatly different constants. Thus, the different binding modes of inhibitors in the functioning and non-functioning complexes are possibly a general characteristic of all IPMDHs.

**pH-dependence of activity of the investigated IPMDHs**

As IPMDH, similar to other oxidative decarboxylases [34], probably functions by the aid of acid-base catalysis, the pH dependence of the enzyme activity is an informative characteristic of the enzyme. We

investigated this property of the *Mtb* IPMDH, and compared it to the other two better-characterised *Tt* and *Ec* IPMDHs. As shown in Fig. 5A, the $k_{cat}$ of *Mtb* IPMDH exhibits a maximum at pH≈9, similar to *Tt* and *Ec* IPMDHs. From analysing the normalised pH vs. activity profiles (Fig. 5B) according to Eq. 1, it became clear that the pH dependence of the activity of *Mtb* IPMDH can be attributed to the dissociation of an ionisable group with p*K*=7.5, similar to *Tt* enzyme (p*K*=7.4), but somewhat different from the pH dependence of *Ec* IPMDH (p*K*=6.7). The larger specific activity of *Ec* IPMDH compared to that of the *Tt* enzyme at pH=7.6 (Table 1) can most probably be attributed to the different pH dependences of their activities (Fig. 5). Since the CD spectra of the enzymes (recorded in the pH range of 6 and 9, not shown) do not indicate the occurrence of any significant structural changes, the observed pH dependences of the activities can most probably be attributed to the ionisation curves of at least one (or more) specific active site residue(s). Site-directed mutagenesis studies with *Tt* IPMDH are underway in our laboratory and are expected to identify the catalytic residue(s) responsible for the observed pH-dependence.

**Denaturation and renaturation experiments with *Mtb* IPMDH**

The spectral changes observed in the protein fluorescence of *Mtb* IPMDH upon ~1 hour incubation in the presence of 8 M urea are shown in Fig. 6A. During denaturation, there is a considerable decrease in the emitted fluorescence intensity with a redshift of the $\lambda_{max}$ from 330 nm to 353 nm. These changes are very similar to those observed previously for the *Tt* and *Ec* IPMDHs [9]. The time dependences of these spectral changes upon denaturation of the *Mtb* IPMDH have been registered and shown in Figs. 6B and 6C, respectively. The half-times of denaturation as derived from these curves are compared to those for *Tt* and *Ec* IPMDHs in Table 2. It is clear that the stability properties of *Mtb* IPMDH resemble more the behaviour of the similarly mesophilic *Ec* IPMDH.

We have also monitored urea-denaturation of *Mtb* IPMDH in the presence of the substrate, IPM. Substrate binding, in addition to the effect of stabilising the catalytically competent protein conformation (e.g. the domain-closed form of IPMDH), in general, can also stabilize the protein structure against the damage caused by denaturing agents. We have reported that binding of MnIPM markedly reduces the rates of unfolding of IPMDHs and this effect is more prominent for the less stable enzyme variants. It is only marginal in case of the thermostable *Tt* IPMDH but pronounced in the cases of the mesophilic *Ec* and the psychrotrophic *Vibrio* sp. I5 IPMDHs [9]. Here, the denaturation experiment with *Mtb* IPMDH in the presence of MnIPM yielded a coherent result (Figs. 6B and 6C). It is clear from Table 2 that the rate of denaturation is slowed down

significantly in the presence of MnIPM, similarly to the case of the other mesophilic form, *Ec* IPMDH. Thus, the protecting effect of the substrate on the protein structure against denaturation correlates well with the structural flexibilities of the various IPMDHs [8, 35].

Refolding kinetics of the denatured *Mtb* IPMDH was recorded by measuring the change of the fluorescence intensity of the protein-bound hydrophobic probe ANS upon decreasing of urea-concentration by dilution. An immediate increase of the ANS fluorescence emission within the mixing time was observed (the fluorescence of ANS bound either to the denatured or the native protein are negligible). This increase is generally characteristic of the formation of a molten globule state, i.e. an intermediate with relatively loosely packed globular structure with the majority of the secondary structural elements formed, but without the rigid tertiary structure [36, 37]. This immediate increase of fluorescence intensity is followed by a slower decrease reflecting the formation of the protein native structure having low affinity for ANS (Fig. 7A). This decrease can be approximated by a single exponential with a rate constant of 0.29±0.07 $min^{-1}$. However, the total change was much smaller (around 10-15%) for *Mtb* IPMDH as compared to the other two (*Tt* and *Ec*) IPMDHs (about 60-70 % [9]). Consistent with this finding, the reactivation studies upon renaturation of *Mtb* IPMDH also led to only a very low yield of the active enzyme with a rate constant of 0.18±0.04 $min^{-1}$ (Fig. 7B).

The rate constants of renaturation of *Mtb* IPMDH are about the same magnitude as those of *Tt* and *Ec* IPMDHs (0.12±0.01 $min^{-1}$ and 0.064±0.006 $min^{-1}$ [9]). However, the extent of renaturation of *Mtb* IPMDH was found to be much smaller compared to the other two investigated IPMDHs. We have checked that this different behaviour of *Mtb* IPMDH cannot be due to its somewhat larger hydrophobic molecular surface compared to *Tt* and *Ec* IPMDHs. The hydrophobic fraction of the accessible surface is in the 56-58% range for each one of the three IPMDHs as determined by using the program ALPHASURF [29]. It is possible, therefore, that the greatly different amino acid sequence of *Mtb* IPMDH (cf. below) is associated with an altered folding pathway of this protein and thereby leads to off-pathway irreversible intermediates.

**Structural comparison of *Mtb* IPMDH with IPMDHs of different origins**

Pairwise comparison of the sequences of various IPMDHs has revealed that the sequence of *Mtb* enzyme is rather different from that of any other IPMDHs while the other IPMDHs have smaller differences among them. Sequence comparison of *Mtb* IPMDH with five other bacterial IPMDHs with known crystal structures has revealed that it is only identical in 33-41% with them, while the identities among these other sequences are higher, at least 48-55% (Table 3). The highest agreement (41%) of *Mtb* IPMDH sequence is found

with the *Tt* IPMDH. This observation might be correlated with the closer similarities in the kinetic properties ($k_{cat}$ and the substrate $K_m$) of *Mtb* and *Tt* IPMDHs. Indeed, the sequence alignment of *Mtb* IPMDH with *Tt* and *Ec* IPMDHs has revealed the identity of 40 and 29 non-conserved amino acid residues, respectively (Fig. S1).

In order to look for the possible differences in the three-dimensional structure of *Mtb* IPMDH relative to other IPMDHs that might be due to the observed sequential differences, we have analysed the molecular contacts of the conserved side-chains in the crystal structure of *Mtb* IPMDH, similar to the previous analysis carried out with *Tt* IPMDH [19]. A disturbance of the important contacts of conserved side-chains by the non-conserved side-chains in the structure of *Mtb* IPMDH might be expected. However, no meaningful structural effects could be observed. This can probably be attributed to the fact that in most cases, chemically similar non-conserved side-chains (e.g. Leu/Ile, Phe/His/Pro, Ser/Thr/Asn) replace each other in the structures of various IPMDHs.

In agreement with these findings, we could model the binding of both substrates into the known crystal structure [18] of *Mtb* IPMDH (Fig. 8). As it is seen, almost all conserved substrate binding residues in the crystal structure of substrate-free *Mtb* IPMDH are located in a steric arrangement allowing formation of contacts with both substrates. A few side-chains (e.g. R97 or D275 in *Mtb* enzyme) are exceptions, but their positions are possibly optimised as soon as the substrates are bound. This is illustrated by superimposition of the respective crystal structures of complexes of *Tt* IPMDH with IPM (Fig. 8A) and with NADH (Fig. 8B) onto the *Mtb* IPMDH structure. Furthermore, the contact lists of all other conserved residues, important for domain-domain communications, are very similar for all three IPMDHs investigated here (Table S1).

It is notable, however, that the static pictures derived from the crystal structures are not enough to explain all the fine details reflected in the kinetic properties of the three IPMDHs (e.g. quantitative values of the catalytic constants cf. Table 1) investigated here. Yet, the main features of the catalysis and its structural background are very similar for all IPMDHs. Thus, any designed new inhibitor of *Mtb* IPMDH, as a potential drug against tuberculosis, can be tested with any one of the other IPMDHs. This can reasonably facilitate designing and testing new inhibitors, as unlike the *Mtb* enzyme, the other IPMDHs can generally be produced by simpler expression procedures.

**ABBREVIATIONS**

IPMDH: 3-isopropylmalate dehydrogenase [EC 1.1.1.85]

IPM: threo-D -3-isopropylmalate or (2R,3S), 2-hydroxy-3-(propan-2-yl)butanedioic acid

*Tt: Thermus thermophilus*

*Ec: Escherichia coli*

*Mtb: Mycobacterium tuberculosis*

BD: Blue dextrane (cf. Fig. 1C)

DLS: Dynamic Light Scattering

FRET: Förster resonance energy transfer

**ACKNOWLEDGEMENTS**

The *Mtb* IPMDH gene cloned in the pETM-11 vector was a gift from Manfred S. Weiss (Helmholtz-Zentrum Berlin für Materialien und Energie, Macromolecular Crystallography, Germany). The financial support by the grants OTKA (K 108642, K 105415) of the Hungarian National Research Fund is gratefully acknowledged.

**SUPPORTING MATERIAL**

Figure S1 provides structure-based sequence alignment of *Mtb*, *Tt and Ec* IPMDHs.

Table S1 gives information about the main atomic contacts of the conserved residues in comparison of *Mtb* and *Tt* IPMDHs.

This material is available free of charge via the Internet at http://pubs.acs.org.

**REFERENCES**

[1] Grandoni, J. A.; Marta, P. T.; Schloss, J. V. Inhibitors of branched-chain amino acid biosynthesis as potential antituberculosis agents. J. Antimicrob. Chemother., 1998, 42, 475-482.

[2] Rajasekaran, P.; Seleem, M. N.; Contreras, A.; Purwantini, E.; Schurig, G. G.; Sriranganathan, N.; Boyle, S. M. Brucella abortus strain RB51 leucine auxotroph as an environmentally safe vaccine for plasmid maintenance and antigen overexpression. Appl. Environ. Microbiol., 2008, 74, 7051-7055.

[3] Hondalus, M. K.; Bardarov, S.; Russell, R.; Chan, J.; Jacobs, W. R., Jr.; Bloom, B. R. Attenuation of and protection induced by a leucine auxotroph of Mycobacterium tuberculosis. Infect. Immun., 2000, 68, 2888-2898.

[4] Dean, A. M. & Dvorak, L. The role of glutamate 87 in the kinetic mechanism of Thermus thermophilus isopropylmalate dehydrogenase. Protein Sci., 1995, 4, 2156-2167.

[5] Miyazaki, K.; Kakinuma, K.; Terasawa, H.; Oshima, T. Kinetic analysis on the substrate specificity of 3-isopropylmalate dehydrogenase. FEBS Lett., 1993, 332, 35-36.

[6] Gráczer, É.; Konarev, P. V.; Szimler, T.; Bacsó, A.; Bodonyi, A.; Svergun, D. I.; Závodszky, P.; Vas, M. Essential role of the metal-ion in the IPM-assisted domain closure of 3-isopropylmalate dehydrogenase. FEBS Lett., 2011, 585, 3297-3302.

[7] Gráczer, É.; Lionne, C.; Závodszky, P.; Chaloin, L.; Vas, M. Transient kinetic studies reveal isomerization steps along the kinetic pathway of Thermus thermophilus 3-isopropylmalate dehydrogenase. FEBS J., 2013, 280, 1764-1772.

[8] Závodszky, P.; Kardos, J.; Svingor; Petsko, G. A. Adjustment of conformational flexibility is a key event in the thermal adaptation of proteins. Proc. Natl. Acad. Sci. U. S. A., 1998, 95, 7406-7411.

[9] Gráczer, É.; Varga, A.; Hajdú, I.; Melnik, B.; Szilágyi, A.; Semisotnov, G.; Závodszky, P.; Vas, M. Rates of unfolding, rather than refolding, determine thermal stabilities of thermophilic, mesophilic, and psychrotrophic 3-isopropylmalate dehydrogenases. Biochemistry, 2007, 46, 11536-11549.

[10] Gráczer, É.; Varga, A.; Melnik, B.; Semisotnov, G.; Závodszky, P.; Vas, M. Symmetrical refolding of protein domains and subunits: example of the dimeric two-domain 3-isopropylmalate dehydrogenases. Biochemistry, 2009, 48, 1123-1134.

[11] Hajdú, I.; Szilágyi, A.; Kardos, J.; Závodszky, P. A link between hinge-bending domain motions and the temperature dependence of catalysis in 3-isopropylmalate dehydrogenase. Biophys. J., 2009, 96, 5003-5012.

[12] Imada, K.; Sato, M.; Tanaka, N.; Katsube, Y.; Matsuura, Y.; Oshima, T. Three-dimensional structure of a highly thermostable enzyme, 3-isopropylmalate dehydrogenase of Thermus thermophilus at 2.2 A resolution. J. Mol. Biol., 1991, 222, 725-738.

[13] Wallon, G.; Kryger, G.; Lovett, S. T.; Oshima, T.; Ringe, D.; Petsko, G. A. Crystal structures of Escherichia coli and Salmonella typhimurium 3-isopropylmalate dehydrogenase and comparison with their thermophilic counterpart from Thermus thermophilus. J. Mol. Biol., 1997, 266, 1016-1031.

[14] Imada, K.; Inagaki, K.; Matsunami, H.; Kawaguchi, H.; Tanaka, H.; Tanaka, N.; Namba, K. Structure of 3-isopropylmalate dehydrogenase in complex with 3-isopropylmalate at 2.0 A resolution: the role of Glu88 in the unique substrate-recognition mechanism. Structure, 1998, 6, 971-982.

[15] Hurley, J. H. & Dean, A. M. Structure of 3-isopropylmalate dehydrogenase in complex with NAD+: ligand-induced loop closing and mechanism for cofactor specificity. Structure, 1994, 2, 1007-1016.

[16] Tsuchiya, D.; Sekiguchi, T.; Takenaka, A. Crystal structure of 3-isopropylmalate dehydrogenase from the moderate facultative thermophile, Bacillus coagulans: two strategies for thermostabilization of protein structures. J. Biochem. (Tokyo), 1997, 122, 1092-1104.

[17] Kadono, S.; Sakurai, M.; Moriyama, H.; Sato, M.; Hayashi, Y.; Oshima, T.; Tanaka, N. Ligand-induced changes in the conformation of 3-isopropylmalate dehydrogenase from Thermus thermophilus. J. Biochem. (Tokyo), 1995, 118, 745-752.

[18] Singh, R. K.; Kefala, G.; Janowski, R.; Mueller-Dieckmann, C.; von Kries, J. P.; Weiss, M. S. The high-resolution Structure of LeuB (Rv2995c) from Mycobacterium tuberculosis. J. Mol. Biol., 2005, 346, 1-11.

[19] Gráczer, É.; Merli, A.; Singh, R. K.; Karuppasamy, M.; Závodszky, P.; Weiss, M. S.; Vas, M. Atomic level description of the domain closure in a dimeric enzyme: Thermus thermophilus 3-isopropylmalate dehydrogenase. Mol. Biosyst., 2011, 7, 1646-1659.

[20] Yamada, T.; Akutsu, N.; Miyazaki, K.; Kakinuma, K.; Yoshida, M.; Oshima, T. Purification, catalytic properties, and thermal stability of threo-Ds-3-isopropylmalate dehydrogenase coded by leuB gene from an extreme thermophile, Thermus thermophilus strain HB8. J. Biochem. (Tokyo), 1990, 108, 449-456.

[21] Ohkuri, T. & Yamagishi, A. The effects of mutations at position 253 on the thermostability of the Bacillus subtilis 3-isopropylmalate dehydrogenase subunit interface. J. Biochem., 2007, 141, 791-797.

[22] Pirrung, M. C.; Han, H.; Chen, J. O-Alkyl Hydroxamates as Metaphors of Enzyme-Bound Enolate Intermediates in Hydroxy Acid Dehydrogenases. Inhibitors of Isopropylmalate Dehydrogenase, Isocitrate Dehydrogenase, and Tartrate Dehydrogenase(1). J. Org. Chem., 1996, 61, 4527-4531.

[23] Nango, E.; Yamamoto, T.; Kumasaka, T.; Eguchi, T. Crystal structure of 3-isopropylmalate dehydrogenase in complex with NAD(+) and a designed inhibitor. Bioorg. Med. Chem., 2009, 17, 7789-7794.

[24] de Marco, A.; Deuerling, E.; Mogk, A.; Tomoyasu, T.; Bukau, B. Chaperone-based procedure to increase yields of soluble recombinant proteins produced in E. coli in BMC Biotechnol., 2007, pp. 32, England.

[25] Pace, C. N.; Vajdos, F.; Fee, L.; Grimsley, G.; Gray, T. How to measure and predict the molar absorption coefficient of a protein. Protein Sci., 1995, 4, 2411-2423.

[26] Laemmli, U. K. Cleavage of structural proteins during the assembly of the head of bacteriophage T4., Nature, 1970, 227, 680-685.

[27] Ornstein, L. Disc Electrophoresis. I. Background and Theory., 1964.

[28] Weber, G. & Young, B. Fragmentation of bovine serum albumin by pepsin. I. The origin of the acid expansion of the albumin molecule. J. Biol. Chem., 1964, 239, 1415-1423.

[29] Edelsbrunner, H. & Koehl, P. The weighted-volume derivative of a space-filling diagram. Proc. Natl. Acad. Sci. U. S. A., 2003, 100, 2203-2208.

[30] Krissinel, E. & Henrick, K. Inference of macromolecular assemblies from crystalline state. J. Mol. Biol., 2007, 372, 774-797.

[31] Rostkowski, M.; Olsson, M. H.; Sondergaard, C. R.; Jensen, J. H. Graphical analysis of pH-dependent properties of proteins predicted using PROPKA. BMC Struct. Biol., 2011, 11, 6.

[32] Yoda, E.; Anraku, Y.; Kirino, H.; Wakagi, T.; Oshima, T. Purification and characterization of 3-isopropylmalate dehydrogenase from a thermoacidophilic archaebacterium Sulfolobus sp. strain 7. FEMS Microbiol. Lett., 1995, 131, 243-247.

[33] Suzuki, T.; Inoki, Y.; Yamagishi, A.; Iwasaki, T.; Wakagi, T.; Oshima, T. Molecular and phylogenetic characterization of isopropylmalate dehydrogenase of a thermoacidophilic archaeon, Sulfolobus sp. strain 7. J. Bacteriol., 1997, 179, 1174-1179.

[34] Aktas, D. F. & Cook, P. F. A lysine-tyrosine pair carries out acid-base chemistry in the metal ion-dependent pyridine dinucleotide-linked beta-hydroxyacid oxidative decarboxylases. Biochemistry, 2009, 48, 3565-3577.

[35] Svingor, A.; Kardos, J.; Hajdú, I.; Németh, A.; Závodszky, P. A better enzyme to cope with cold. Comparative flexibility studies on psychrotrophic, mesophilic, and thermophilic IPMDHs. J. Biol. Chem., 2001, 276, 28121-28125.

[36] Semisotnov, G. V.; Rodionova, N. A.; Kutyshenko, V. P.; Ebert, B.; Blank, J.; Ptitsyn, O. B. Sequential mechanism of refolding of carbonic anhydrase B., FEBS Lett., 1987, 224, 9-13.

[37] Semisotnov, G. V.; Rodionova, N. A.; Razgulyaev, O. I.; Uversky, V. N.; Gripas, A. F.; Gilmanshin, R. I. Study of the "molten globule" intermediate state in protein folding by a hydrophobic fluorescent probe. Biopolymers, 1991, 31, 119-128.

**LEGENDS to the FIGURES**

**Fig. 1 Gel electrophoresis and gel filtration of *Mtb* IPMDH-containing samples** In (A) samples for the SDS-PAGE were taken from the fermentor (intact cells) at the end of the fed-batch phase (2), before the induction (3) and 3 hours after the induction (4). The samples were diluted 5 times and 3 μL was loaded into the gel. A sample of 5 μg of purified *Mtb* IPMDH (5) also was loaded into the gel. In (B) native gel electrophoresis of samples of *Tt*, *Mtb* and *Ec* IPMDHs were run as described in the Experimental part. In (C) the results of the Superose 12 gel filtrations are shown. The following protein samples were used for calibration: 1. lysozime (14.4 kDa), 2. chymotrypsinogen A (25 kDa), 3. phosphoglycerate kinase (44.5 kDa), 4. bovine serum albumin (66.4 kDa) and 5. aldolase (160 kDa). The apparent molecular weights of *Tt*, *Ec* and *Mtb* IPMDHs were determined to be 63.6 kDa, 65.5 kDa and 88.6 kDa, respectively. In (D) gel electrophoresis of denaturated *Tt*, *Mtb* and *Ec* IPMDHs is illustrated in the presence of 8 M urea. The *Tt* sample was run both before and after the other samples in order to detect differences, if any, in their running rates, due to any inherent error of the electrophoretic run. A small fraction of the remaining native part of the *Tt* IPMDH is also observable.

**Fig. 2 Modelling of the tetrameric structure of *Mtb* IPMDH** The oligomeric structure of *Mtb* IPMDH was predicted using the X-ray coordinates (pdb 1W0D, [18]) by the aid of PISA server [30]. The subunits within each dimer are illustrated by black and grey ribbon diagrams, respectively. The interacting arms of the subunits are indicated by arrows.

**Fig. 3 Spectral properties of *Mtb* IPMDH as compared to *Tt* and *Ec* IPMDHs** The spectra of *Mtb* (dotted), *Tt* (dashed) and *Ec* (dashed-dot-dot) IPMDHs were recorded by UV absorbance (A). The spectrum of the bound nucleotide (grey solid) was subtracted from the original spectrum of the native *Mtb* IPMDH (dotted), the spectrum of the nucleotide-free *Mtb* IPMDH (black solid line) can be obtained. The spectra of *Mtb* (black solid), *Tt* (dashed) and *Ec* (dashed-dot-dot) IPMDHs were also recorded by far-UV CD (B), protein fluorescence emission (C) and fluorescence resonance energy transfer (D). Protein concentrations of 0.6 mg/mL (15 μM monomer) and 12 μg/mL (0.32 μM monomer) were applied in CD (B) and fluorescence (C and D) measurements, respectively. The excitation was carried out at 295 nm and the excitation and emission slits were 2-4 nm in (C and D).

**Fig. 4 Characterization of the inhibitor (2S,3S)-(-)-2-hydroxy-3-sulfanylbutanedioic acid** The inhibitory effect of (2S,3S)-(-)-2-hydroxy-3-sulfanylbutanedioic acid (or 3-methylmercaptomalate) on *Mtb* (△) and *Tt* (○) IPMDHs is illustrated by a Lineweaver-Burk plot (A). The activities were recorded in the absence and in the presence of 37 μM inhibitor. The competitive inhibitory constant ($K_I$) values are obtained to be 427±50 nM and 349±50 nM, respectively, for *Mtb* and *Tt* IPMDHs. 3-methylmercaptomalate binding to the complex of native IPMDH-NADH binary complex was monitored by recording the appearance of the FRET signal (B) upon addition of increasing concentration of 3-methylmercaptomalate to *Mtb* (△, right axis) and *Tt* (○, left axis) IPMDHs. The $K_d$ values of 87±15 μM and 178±20 μM were derived for *Mtb* and *Tt* IPMDHs, respectively, by fitting the experimental data to Eq. 2 (cf. Experimental part).

**Fig. 5 The pH dependence of the activity ($k_{cat}$) of IPMDHs**

The enzyme activities of *Mtb* (△), *Tt* (○) and *Ec* (□) IPMDHs were determined at the protein concentration 6 μg/mL (0.16 μM monomer) at different pH values (A). On panel (B) the pH dependence curves are normalised to the *Tt* enzyme. The data were fitted by a bell-shaped curve in accordance with the Eq. 1. The pH dependence of activity of *Mtb* IPMDH can be attributed to dissociation of an ionisable group with p*K*=7.5, similar to *Tt* enzyme (p*K*=7.4), but somewhat different from the pH-dependence of *Ec* IPMDH (p*K*=6.7).

**Fig. 6 Denaturation of *Mtb* IPMDH as followed by protein fluorescence** The spectral changes accompanying the denaturation of *Mtb* IPMDH are represented by the spectra of the native (solid line) and denaturated (dashed line) enzymes (A). During denaturation the emission spectra were recorded in the presence (●) and in the absence (△) of IPM in every 5 minutes. The values of $\lambda_{max}$ (B) and the fluorescence intensities at 335 nm (C) were plotted at different time intervals during denaturation. The half time of 8.6±1 and 29.9±5 min were obtained by fitting the curves to a single exponential.

**Fig. 7 Renaturation time courses of *Mtb* IPMDH** Refolding kinetic curves of *Mtb* IPMDH was determined by recording the changes of the bound ANS fluorescence (A) and enzyme activity (B). The protein concentrations were 6 μg/mL (0.16 μM monomer) (A) and 60 μg/mL (1.6 μM monomer) (B). The corresponding rate constants are 0.29±0.07 and 0.18±0.04 $min^{-1}$.

**Fig. 8 Demonstration of the similar active site architectures of *Mtb* and *Tt* IPMDHs: IPM (A) and NADH (B) binding** The *Tt* (grey, pdb entries 2Y41 and 2Y42 for the IPM and NADH bound complexes, respectively, [19]) and *Mtb* (black, pdb 1W0D, [18]) IPMDH structures were superimposed by the secondary structural elements of the Domain 2 (A) or Domain 1 (B), respectively. The conserved side-chains involved in the substrate binding are represented by stick models. The substrates MnIPM and NADH are illustrated by ball-and-stick models, respectively. The dashed lines represent atomic interactions of *Tt* IPMDH with the substrates.

# Fig. 1

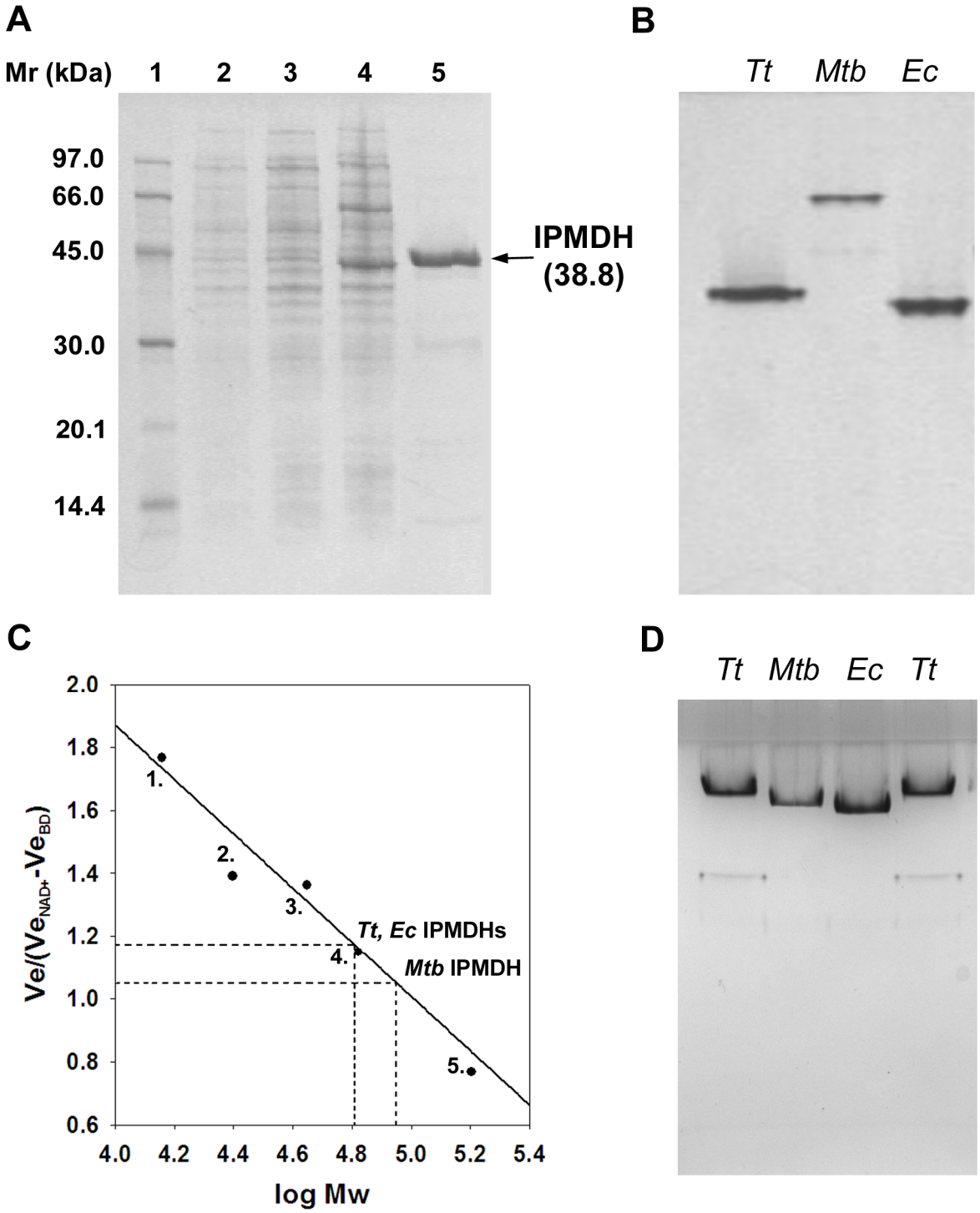
A
Mr (kDa)
1
2
3
4
5
97.0
66.0
45.0
30.0
20.1
14.4
IPMDH
(38.8)
B
Tt
Mtb
Ec
C
Ve/(Ve$_{NAD+}$-Ve$_{BD}$)
2.0
1.8
1.6
1.4
1.2
1.0
0.8
0.6
1.
2.
3.
4.
5.
Tt, Ec IPMDHs
Mtb IPMDH
4.0
4.2
4.4
4.6
4.8
5.0
5.2
5.4
log Mw
D
Tt
Mtb
Ec
Tt

# Fig. 2

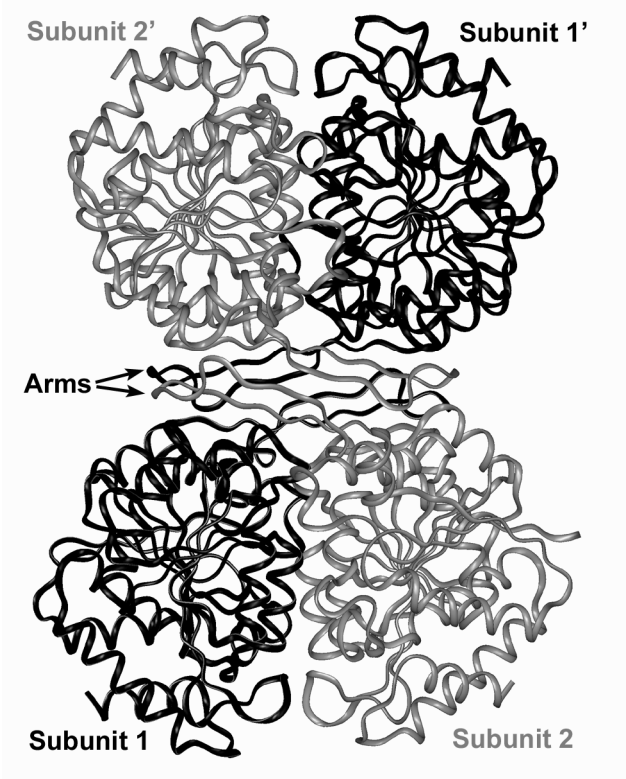

# Fig. 3

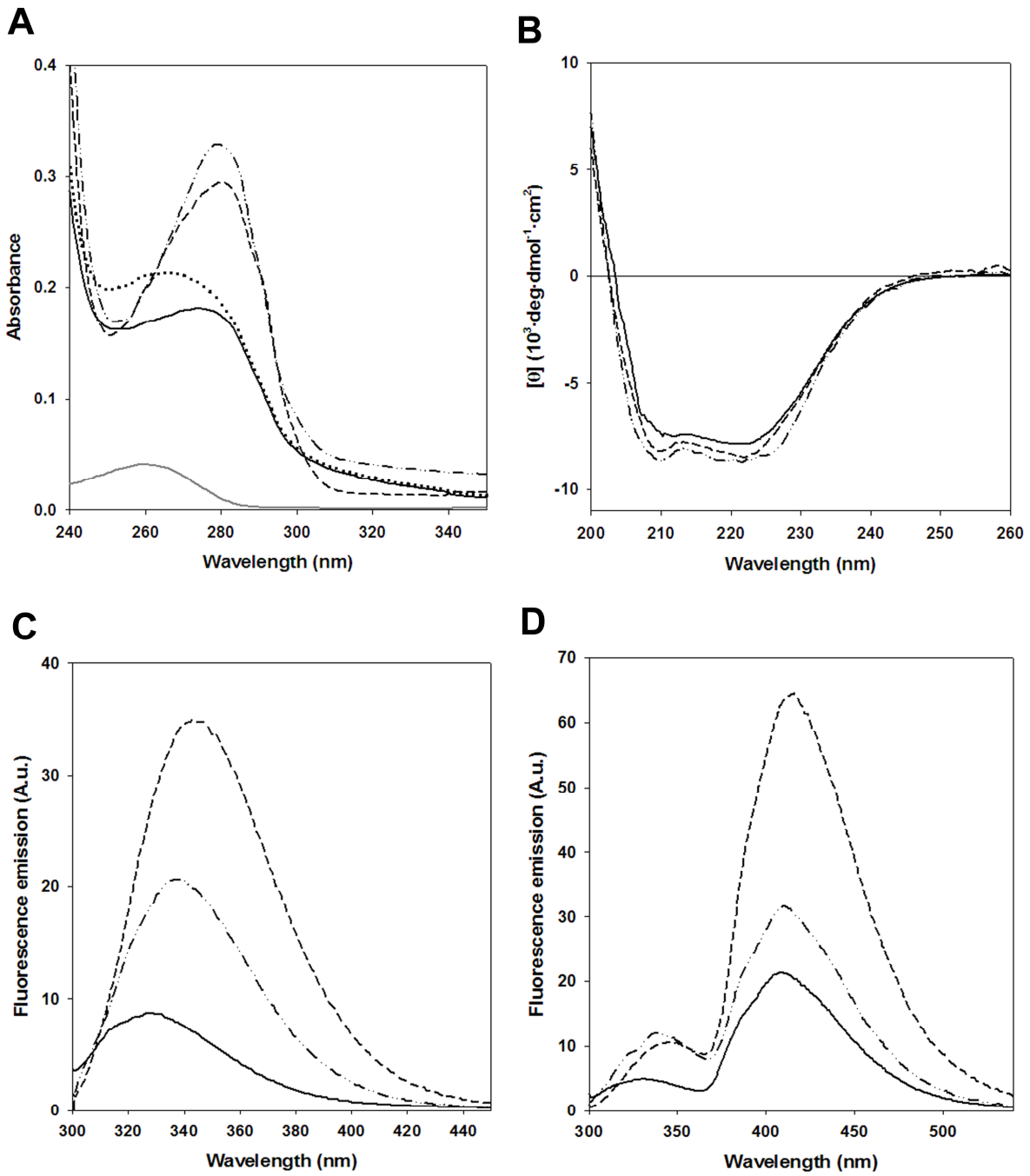
A
Absorbance
Wavelength (nm)
B
[θ] (10³·deg·dmol⁻¹·cm²)
Wavelength (nm)
C
Fluorescence emission (A.u.)
Wavelength (nm)
D
Fluorescence emission (A.u.)
Wavelength (nm)

# Fig. 4

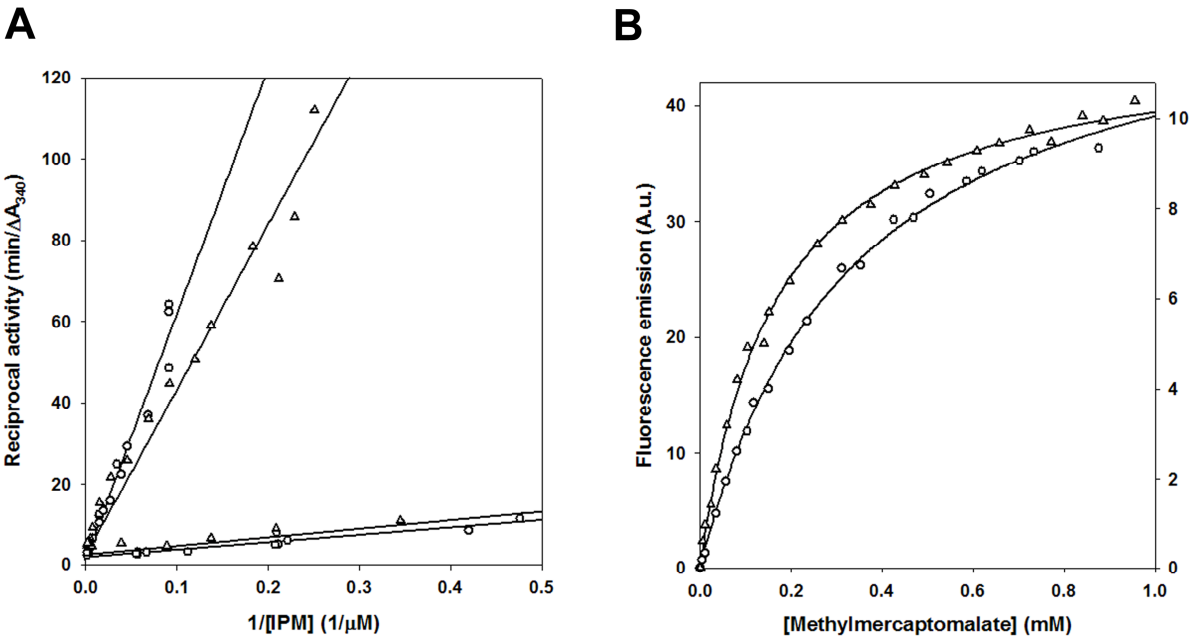
A
B
Reciprocal activity (min/ΔA340)
1/[IPM] (1/μM)
Fluorescence emission (A.u.)
[Methylmercaptomalate] (mM)

# Fig. 5

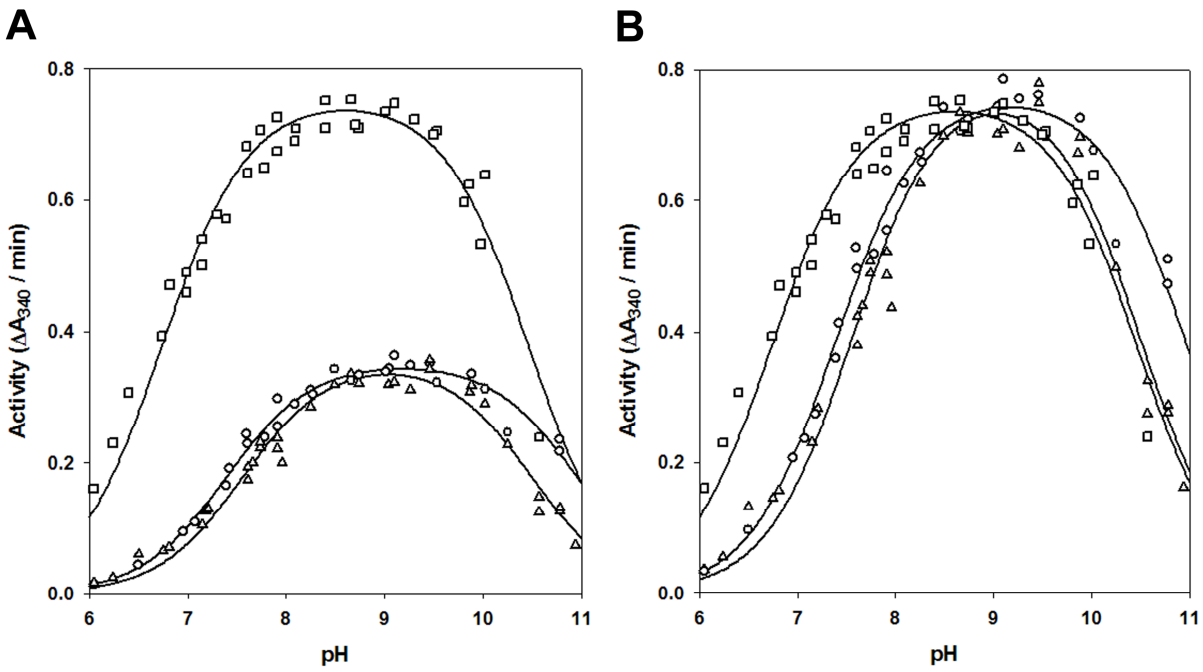

# Fig. 6

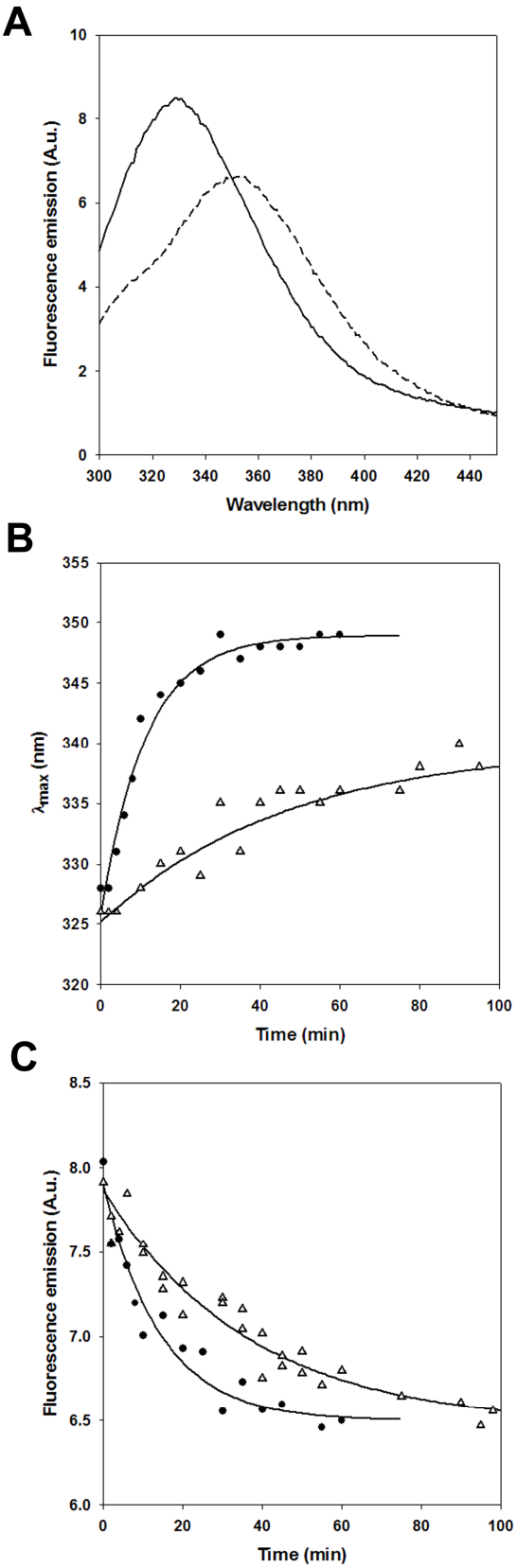
A
Fluorescence emission (A.u.)
Wavelength (nm)
B
λmax (nm)
Time (min)
C
Fluorescence emission (A.u.)
Time (min)

# Fig. 7

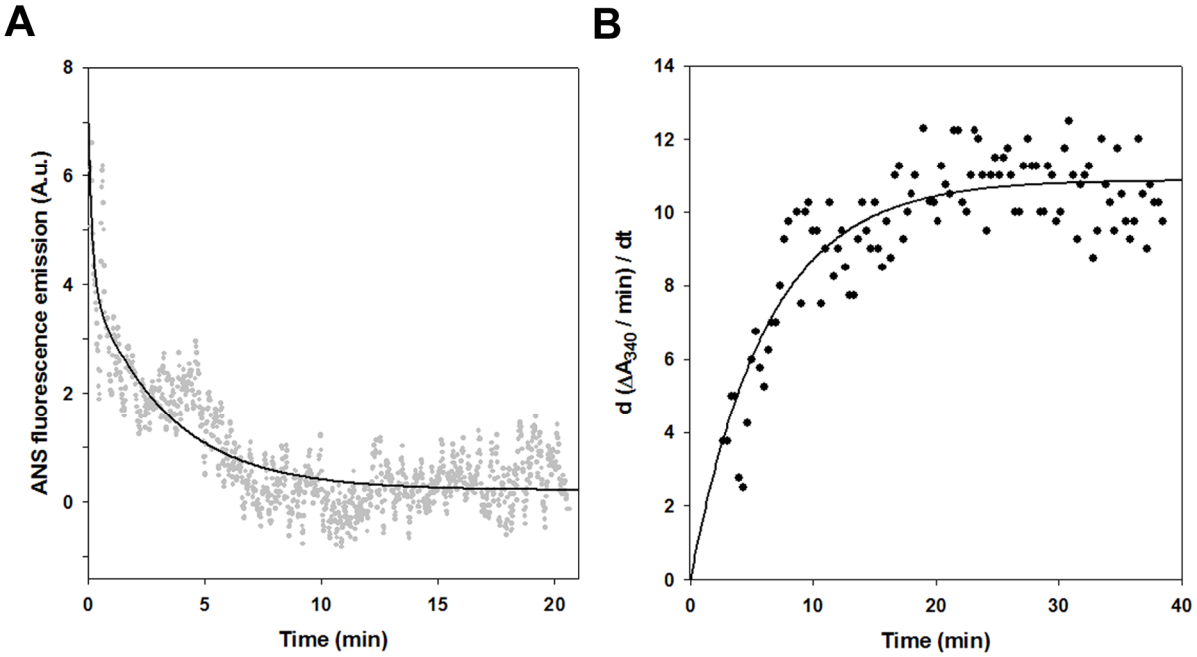
A
B
ANS fluorescence emission (A.u.)
Time (min)
d (ΔA340 / min) / dt
Time (min)

# Fig. 8

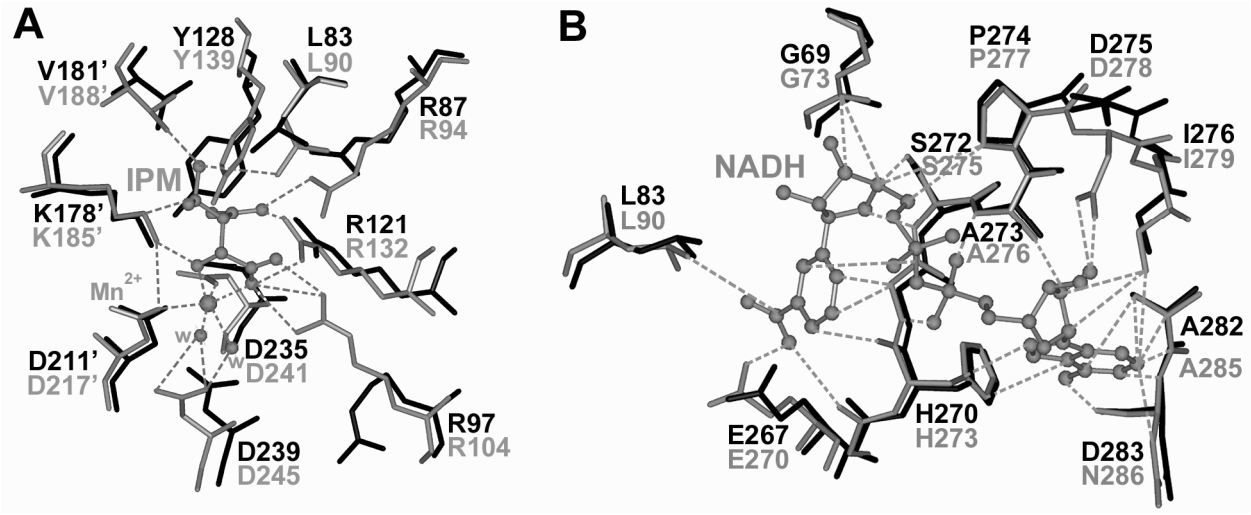
A
Y128
Y139
L83
L90
V181'
V188'
R87
R94
IPM
K178'
K185'
R121
R132
Mn2+
w
D211'
D217'
w
D235
D241
R97
R104
D239
D245
B
G69
G73
P274
P277
D275
D278
I276
I279
NADH
S272
S275
L83
L90
A273
A276
A282
A285
H270
H273
E267
E270
D283
N286

**Table 1 Comparison of the kinetic parameters and substrate binding constants of the three different IPMDHs at pH=7.6** The kinetic and binding experiments are described in the Methods section.

| IPMDH | $K_m$ (μM) | | | $k_{cat}$ ($min^{-1}$) | $\frac{k_{cat}}{K_{m,IPM}}$ ($M^{-1}min^{-1}$) | $K_{d,IPM}$ (μM) |
|---|---|---|---|---|---|---|
| | IPM | $NAD^+$ | $Mn^{2+}$ | | | |
| ***Myc*** | 5.8±2 | 134±30 | 15±5 | 200±20 | $(3.45±1.3)\cdot 10^7$ | 5.3±2 |
| ***Tt*** | 16.0±5 | 328±50 | 10.2±3 | 238±30 [a] | $(1.51±0.6)\cdot 10^7$ | 17.0±4 |
| ***Ec*** | 4.9±2 | 159±25 | 17.6±4 | 700±80 [a] | $(1.43±0.5)\cdot 10^8$ | 5.5±2 |

[a] Ref. [6].

**Table 2 Protective effect of the substrate MnIPM against denaturation of the investigated IPMDHs** The half time of urea-denaturation ($t_{1/2}$, min) was determined in the absence and presence of MnIPM.

| IPMDH | No IPM ($t_{1/2}$, min) | With IPM ($t_{1/2}$, min) |
|---|---|---|
| ***Mtb*** | 8.6±3 | 29.9±5 |
| ***Tt*** [a] | 46.2±8 | 53.3±8 |
| ***Ec*** [a] | 5.0±2 | 30.1±7 |

[a] Denaturation of these enzymes were studied earlier [9].

**Table 3 Sequential comparison of various IPMDHs** Percentage of the identical amino acid residues are indicated in pairwise comparisons of the alighned sequences.

| | ***Mtb*** | ***Thermotoga maritima*** | ***Thiobacillus ferrooxidans*** | ***Ec*** | ***Salmonella typhimurium*** | ***Tt*** |
|---|---|---|---|---|---|---|
| ***Tt*** | **40.9 %** | **53.5 %** | **52.8 %** | **48.8 %** | **47.9 %** | **100 %** |
| ***Salmonella typhimurium*** | **37.2 %** | **55.2 %** | **48.9 %** | **94.5 %** | **100 %** | |
| ***Ec*** | **37.2 %** | **55.5 %** | **49.5 %** | **100 %** | | |
| ***Thiobacillus ferrooxidans*** | **38.9 %** | **50.8 %** | **100 %** | | | |
| ***Thermotoga maritima*** | **37.5 %** | **100 %** | | | | |
| ***Mtb*** | **100 %** | | | | | |

# SUPPORTIVE MATERIAL

**Drugs against *Mycobacterium tuberculosis* 3-isopropylmalate dehydrogenase can be developed using homologous enzymes as surrogate targets**

Éva Gráczer, András Bacsó, Dénes Kónya, Adrián Kazi, Tibor Soós, Laura Molnár, Tamás Szimler, László Beinrohr, András Szilágyi, Péter Závodszky and Mária Vas

**Fig. S1 Structure-based sequence alignment of IPMDHs of different origins** The 46 conserved residues are marked with a single asterisk. Double asterisks mark the 18 residues that directly interact with the substrates. The locations of secondary structure elements are labelled with arrows. The non-conserved residues that are identical in *Mtb* and *Tt* IPMDHs, as well as in *Mtb* and *Ec* structures are highlighted by black and grey backgrounds, respectively.

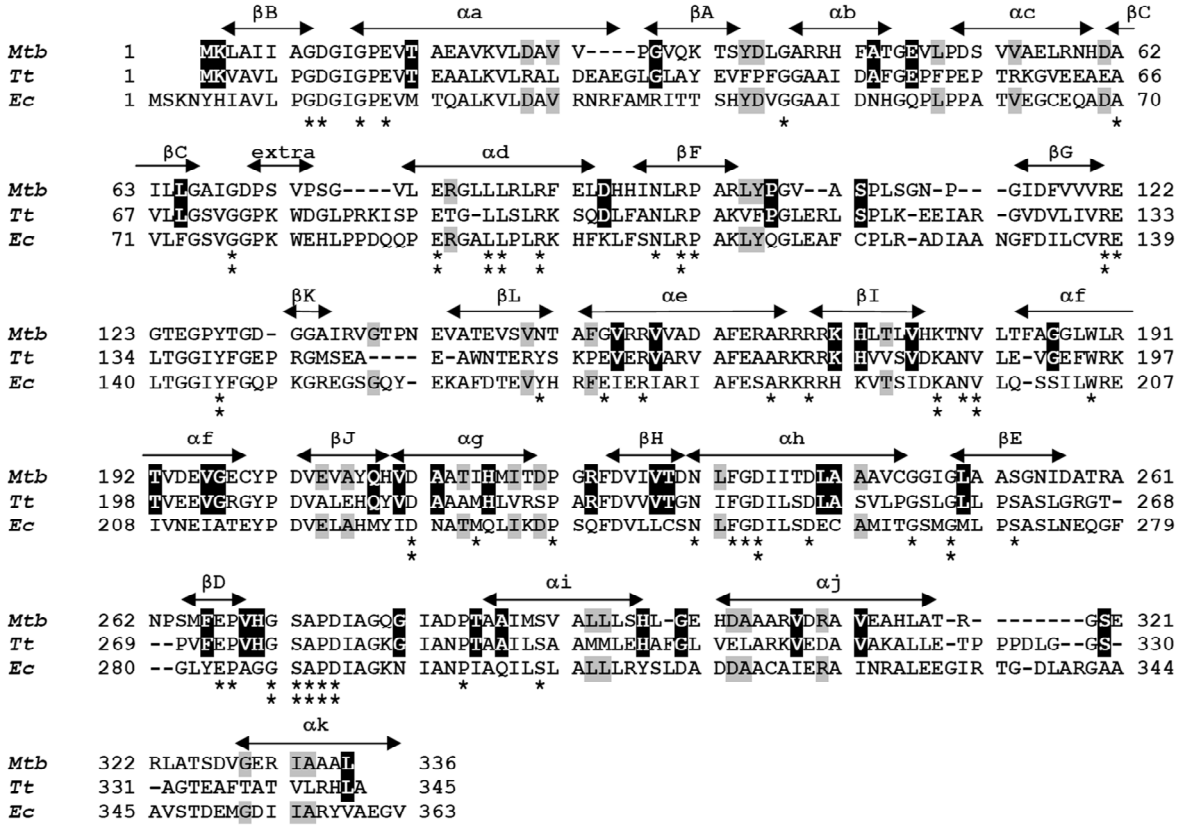

**Table S1 The main atomic contacts of the conserved residues in comparison of *Mtb* and *Tt* IPMDHs** The list of the atomic distances has been derived from the crystal structures of *Mtb* and *Tt* IPMDHs (pdb codes 1W0D and 2Y41, respectively).

| ***Mtb* IPMDH** | | | | | ***Tt* IPMDH** | | | | |
|---|---|---|---|---|---|---|---|---|---|
| Side-chain | Atom1 | Side-chain | Atom2 | Distance (Å) | Side-chain | Atom1 | Side-chain | Atom2 | Distance (Å) |
| Asp9 | OD2 | Gly69 | N | 2.83 | Asp9 | OD2 | Gly73 | N | 2.88 |
| | CB | Ser272 | CB | 4.25 | | CB | Ser275 | CB | 4.34 |
| | C | | CB | 3.88 | | C | | CB | 3.90 |
| Gly12 | CA | Gly66 | CA | 4.18 | Gly12 | CA | Gly70 | CA | 4.36 |
| Glu14 | CD | Gly278 | CA | 3.61 | Glu14 | CD | Gly281 | CA | 4.04 |
| Ala62 | N | Lys2 | O | 3.58 | Ala66 | N | Lys2 | O | 2.87 |
| Arg87 | NH1 | Glu267 | OE2 | 4.86 | Arg94 | NH2 | Glu270 | OE2 | 2.95 |
| His93 | CG | Arg157 | CZ | 3.37 | Phe100 | CG | Arg164 | CZ | 3.75 |
| | CG | | CD | 4.02 | | CG | | CD | 3.76 |
| | CD2 | | CG | 4.64 | | CD2 | | CG | 4.40 |
| | CD2 | | CD | 3.87 | | CD2 | | CD | 3.74 |
| | CD2 | | CZ | 4.05 | | CD2 | | CZ | 3.61 |
| | CE1 | | CD | 4.06 | | CE1 | | CD | 4.05 |
| | CE1 | | CZ | 3.88 | | CE2 | | CZ | 4.40 |
| Asn95 | O | Arg121 | N | 2.79 | Asn102 | N | Arg132 | O | 2.94 |
| | N | | O | 2.75 | | O | | N | 2.81 |
| | CB | | CB | 4.05 | | CB | | CB | 4.04 |
| Arg97 | CD | Thr238 | CB | 4.28 | Arg104 | CB | Ser244 | CB | 3.47 |
| | NH2 | Asp239 | OD1 | 4.76 | | NH1 | Asp241 | OD1 | 4.49 |
| Pro98 | CD | Ala252 | C | 4.23 | Pro105 | CD | Pro258 | C | 4.26 |
| Arg121 | NH1 | Asn231 | OD1 | 2.91 | Arg132 | NH1 | Asn237 | OD1 | 4.49 |
| | CB | Gly234 | CA | 3.99 | | CB | Gly240 | CA | 4.26 |
| | CB | | C | 4.49 | | CB | | C | 4.48 |
| | NH1 | Asp235 | OD1 | 3.50 | | NH1 | Asp241 | OD1 | 3.90 |
| | NH2 | | OD1 | 3.62 | | NH2 | | OD1 | 4.22 |
| | CZ | | CB | 3.70 | | CZ | | CB | 3.78 |
| Glu122 | O | Asn231 | ND2 | 3.25 | Glu133 | O | Asn237 | ND2 | 3.47 |
| | C | | CB | 4.10 | | C | | CB | 4.33 |
| | C | | CG | 4.09 | | C | | CG | 4.14 |
| Tyr128 | CB | | CG | 4.01 | Tyr139 | CB | | CG | 4.11 |
| | CG | | CG | 4.53 | | CG | | CG | 3.73 |
| | CD2 | | CG | 4.21 | | CD2 | | CG | 3.95 |
| Tyr128 | OH | Asp235 | OD2 | 3.48 | Tyr139 | OH | Asp241 | OD2 | 3.43 |
| | CZ | | CB | 4.31 | | CZ | | CB | 4.43 |
| Arg169 | NH2 | Asp225 | OD1 | 2.92 | Arg176 | NH2 | Asp231 | OD1 | 3.11 |
| | NE | | OD1 | 2.64 | | NE | | OD1 | 2.68 |
| | NE | | OD2 | 4.37 | | NE | | OD2 | 4.41 |
| | CB | | CG | 3.97 | | CB | | CG | 3.86 |
| Lys178 | O | Asn180 | N | 3.13 | Lys185 | O | Asn187 | N | 3.30 |
| | O | Val181 | N | 3.28 | | O | Val188 | N | 3.13 |
| | NZ | Asp211 | OD1 | 3.22 | | NZ | Asp217 | OD1 | 3.58 |
| | NZ | | OD2 | 3.32 | | NZ | | OD2 | 3.25 |
| | CB | Phe233 | CZ | 3.62 | | CB | Phe239 | CZ | 4.19 |
| | CB | Phe233 | CE2 | 3.92 | | CB | Phe239 | CE2 | 4.24 |
| Gly249 | CA | His270 | CD2 | 4.35 | Gly255 | CA | His273 | CD2 | 4.06 |
| Glu267 | CA | Ser290 | CB | 3.74 | Glu270 | CA | Ser293 | CB | 4.24 |
| | C | | CB | 3.37 | | C | | CB | 4.02 |
| | N | | OG | 3.69 | | O | | OG | 3.28 |
| Pro268 | N | | OG | 3.94 | Pro271 | N | | OG | 3.30 |
| Ser272 | CB | Gly69 | C | 4.28 | Ser275 | CB | Gly73 | C | 4.22 |
| Pro284 | CB | Val15 | CA | 4.05 | Pro287 | CB | Val15 | CA | 4.47 |
| Ser290 | CB | Phe266 | C | 4.03 | Ser293 | CB | Phe269 | C | 4.13 |

For Table of Contents Use Only

**Drugs against *Mycobacterium tuberculosis* 3-isopropylmalate dehydrogenase can be developed using homologous enzymes as surrogate targets**

Éva Gráczer, András Bacsó, Dénes Kónya, Adrián Kazi, Tibor Soós, Laura Molnár, Tamás Szimler, László Beinrohr, András Szilágyi, Péter Závodszky and Mária Vas